Tropical Cold-Point Tropopause: Climatology, Seasonal Cycle, and Intraseasonal Variability Derived from COSMIC GPS Radio Occultation Measurements

JOOWAN KIM AND SEOK-WOO SON

Department of Atmospheric and Oceanic Sciences, McGill University, Montreal, Quebec, Canada

(Manuscript received 29 September 2011, in final form 1 February 2012)

ABSTRACT

The finescale structure of the tropical cold-point tropopause (CPT) is examined using high-resolution temperature profiles derived from Constellation Observing System for Meteorology, Ionosphere and Climate (COSMIC) global positioning system (GPS) radio occultation measurements for 4 yr from September 2006 to August 2010. The climatology, seasonal cycle, and intraseasonal variability are analyzed for three CPT properties: temperature (T-CPT), pressure (P-CPT), and sharpness (S-CPT). Their relationships with tropospheric and stratospheric processes are also discussed.

The climatological P-CPT is largely homogeneous in the deep tropics, whereas T-CPT and S-CPT exhibit local minima and maxima, respectively, at the equator in the vicinity of deep convection regions. All three CPT properties, however, show coherent seasonal cycle in the tropics; the CPT is colder, higher (lower in pressure), and sharper during boreal winter than during boreal summer. This seasonality is consistent with the seasonal cycle of tropical upwelling, which is largely driven by stratospheric and near-tropopause processes, although the amplitude of the seasonal cycle of T-CPT and S-CPT is modulated by tropospheric circulations. On intraseasonal time scales, P-CPT and T-CPT exhibit homogeneous variability in the deep tropics, whereas S-CPT shows pronounced local variability and seasonality. The wavenumber–frequency spectra reveal that intraseasonal variability of CPT properties is primarily controlled by Kelvin waves, with a nonnegligible contribution by Madden–Julian oscillation convection. The Kelvin waves, which are excited by deep convection but often propagate along the equator freely, explain the homogeneous P-CPT and T-CPT variabilities. On the other hand, the vertically tilted dipole of temperature anomalies, which is associated with convectively coupled equatorial waves, determines the local structure and seasonality of S-CPT variability.

1. Introduction

In the tropics, the thermal boundary between the stratosphere and troposphere is well defined by the coldest level, the so-called cold-point tropopause (CPT). Thermal characteristics of the CPT have been extensively examined as they play a crucial role in stratosphere–troposphere coupling and exchange (Holton et al. 1995). For instance, transport of water vapor from the troposphere to the stratosphere is to a great extent controlled by temperature at the CPT. Because the air that enters the stratosphere through the tropical tropopause undergoes a freeze-drying process near the CPT (Brewer 1949), the amount of water vapor transported into the stratosphere is highly dependent on thermal characteristics of the CPT (Holton et al. 1995; Mote et al. 1996). It is known that small changes in water vapor in the stratosphere can drive significant changes in the climate below by modifying the global radiation budget (Holton et al. 1995; de F. Forster and Shine 1999). Because of this climate effect, the CPT has received much attention in the recent past (Solomon et al. 2010; Gettelman et al. 2010).

The physical properties of the CPT have been examined using observations (Seidel et al. 2001; Zhou et al. 2001a; Randel et al. 2003), reanalysis data (Zhou et al. 2001b; Gettelman et al. 2002b; Fueglistaler et al. 2009), and climate model output (Gettelman and Birner 2007; Gettelman et al. 2009). It is now well known that temperature of the CPT (T-CPT) is at a minimum over the western Pacific (WP; Randel et al. 2000; Seidel et al. 2001; Randel et al. 2003), with secondary minima over the eastern Pacific and western Africa, whereas pressure of the CPT (P-CPT) has a relatively weak longitudinal structure. Both T-CPT and P-CPT undergo a strong seasonal cycle, with a colder T-CPT and lower P-CPT

Corresponding author address: Joowan Kim, Department of Atmospheric and Oceanic Sciences, McGill University, 805 Sherbrooke Street West, Montreal QC H3A 2K6, Canada.
E-mail: joowan.kim@mail.mcgill.ca

DOI: 10.1175/JCLI-D-11-00554.1

during boreal winter than during boreal summer. This seasonality has been related to the seasonal cycle of the stratospheric Brewer–Dobson circulation (Yulaeva et al. 1994) and recently to tropical and extratropical waves acting near the tropical tropopause (Kerr-Munslow and Norton 2006; Norton 2006; Randel et al. 2008). In contrast to the seasonal cycle, intraseasonal variability of CPT properties is known to be associated with convective activity in the tropics (Zhou and Holton 2002; Randel et al. 2003; Randel and Wu 2005). Using reanalysis data, Zhou and Holton (2002) showed the temporal evolution of T-CPT to have a clear correspondence with Madden–Julian oscillation (MJO) convection and Kelvin wave activities. From observations, Randel et al. (2003) also showed an example of organized temperature response, in the upper troposphere and lower stratosphere (UTLS), to tropical convection at intraseasonal time scales. The long-term variability and trend of T-CPT have also been examined. Randel et al. (2000) and Zhou et al. (2001b) investigated the interannual variability of T-CPT using radiosonde and reanalysis data and reported its relation with the quasi-biennial oscillation (QBO) and El Niño–Southern Oscillation (ENSO). Seidel et al. (2001), Zhou et al. (2001a), and Solomon et al. (2010) further showed that T-CPT has cooled during recent decades.

However, it should be noted that, in spite of extensive previous studies, the detailed characteristics of CPT properties still remain ambiguous. This is to a large degree due to the lack of observations in the UTLS. Most of aforementioned studies are in fact based on radiosonde and reanalysis data. These data have either limited spatial coverage or low vertical resolution in the UTLS. Particularly, CPT analyses using reanalysis data assume a fixed pressure level for the CPT (generally 100 hPa), being unable to capture the temperature and pressure variations of the CPT accurately. Zhou et al. (2001a) reported that CPT analysis using reanalysis data could introduce a warm temperature bias of about 2 K, a high pressure bias of about 7 hPa, and a corresponding overestimation of saturation water vapor mixing ratio by about 1.3 ppmv.

More reliable observational analyses have recently been enabled by global positioning system (GPS) radio occultation measurements. The GPS measurements provide very accurate temperature profiles over the globe with relatively high vertical resolution. Using temperature profiles derived from the GPS/Meteorology (GPS/MET) mission, Nishida et al. (2000) and Randel et al. (2003) showed that the accuracy of the temperature profiles from GPS radio occultation measurements is quantitatively similar to that of radiosonde observations in the UTLS region. They also demonstrated that GPS radio occultation measurements are very useful for examining thermal structure and variability of the CPT as later examined in detail by Schmidt et al. (2004) using Challenging Minisatellite Payload (CHAMP) data and Kishore et al. (2006) using CHAMP and Satellite de Aplicaciones Cientificas-C (SAC-C) data.

By extending and updating these studies, here we examine physical properties of the CPT from the newly available GPS observations: the Constellation Observing System for Meteorology, Ionosphere and Climate (COSMIC) GPS radio occultation measurements (Anthes et al. 2008). The COSMIC mission provides a large number of temperature profiles with superior spatial coverage compared to other GPS missions because it utilizes a six-satellite constellation. This feature allows us to examine finescale structure of CPT properties and their high-frequency variabilities. In particular, we examine climatology, seasonal cycle, and intraseasonal variability of three CPT properties (temperature, pressure, and sharpness) as in Son et al. (2011), where lapse rate tropopause properties were analyzed using COSMIC data. The observed characteristics are then discussed in connection with dynamical and thermodynamical processes in the UTLS.

This paper is organized as follows: The data and method used in this study are described in section 2. Section 3 presents the climatology of CPT properties. Sections 4 and 5 investigate the seasonal cycle and intraseasonal variability of the CPT, respectively. A summary and discussion are given in section 6.

2. Data and method

CPT properties are examined using dry temperature profiles[1] derived from COSMIC GPS radio occultation measurements. The COSMIC mission provides approximately 1800 temperature profiles per day over the globe with relatively high vertical resolution, of which about 500 profiles are located in the tropics (30°S–30°N). Figure 1 shows the number of temperature profiles per month in the tropics and deep tropics. Although data are available from April 2006, we use 4 yr of data from September 2006 to August 2010, because the number of temperature profiles during the first few months is relatively small. Based on geometric optics, the typical vertical resolution of the GPS radio occultation measurements is about 1 km at the tropopause (Kursinski et al. 1997). However, this resolution can be increased up to 100 m with the use of advanced technique, such

[1] CPT properties were examined also using temperature profiles retrieved without a dry-atmosphere assumption (the so-called wet profiles), and no qualitative difference was found in the analysis.

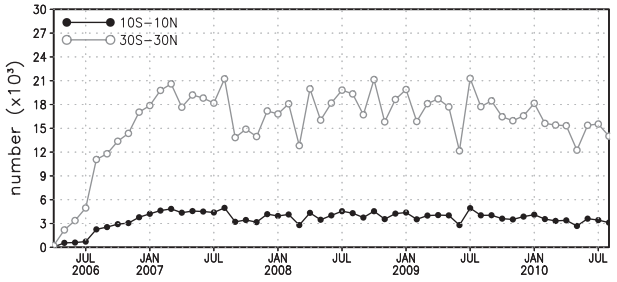

FIG. 1. Number of COSMIC GPS radio occultation soundings per month from April 2006 to August 2010.

as a wave-optics method (e.g., Jensen et al. 2003; Gorbunov and Lauritsen 2004), which is partly employed in the COSMIC mission. Because the maximum resolution varies in time and space, all temperature profiles are vertically interpolated onto 200-m intervals for simplicity. Each CPT property is computed using this interpolated data and then gridded into 5° × 5° (longitude × latitude) non-overlapping grid boxes. The mean data density is roughly 18 profiles per grid box per month.

To evaluate the CPT properties derived from the COSMIC measurements, we also analyze radiosonde observations archived at the Integrated Global Radiosonde Archive (IGRA; Durre et al. 2006). National Oceanic and Atmospheric Administration (NOAA) outgoing longwave radiation (OLR) (Liebmann and Smith 1996) and European Centre for Medium-Range Weather Forecasts (ECMWF) Interim Reanalysis (ERA-Interim; Simmons et al. 2007) data are also used to compliment the information of convection and background flow. Here, ERA-Interim is selected because it assimilates COSMIC data.

Three CPT properties are examined in this study: T-CPT, P-CPT, and CPT sharpness (S-CPT). T-CPT and P-CPT are defined as the coldest temperature and its pressure between 300- and 50-hPa levels. S-CPT is defined as the static stability (measured by the square of buoyancy frequency N^2) change across the CPT,

$$\text{S-CPT} = N_+^2 - N_-^2 \quad \text{and} \tag{1}$$

$$N^2 = \frac{g}{T}\left(\frac{g}{c_p} + \frac{\partial T}{\partial z}\right),$$

where N_+^2 and N_-^2 denote N^2 averaged from the CPT to 1 km above and below, respectively. All other symbols have standard meanings. Although not shown, this definition gives a qualitatively similar result to the sharpness defined as lapse rate change (e.g., Schmidt et al. 2004). In Eq. (1), S-CPT is dominated by N_+^2, which is often used to quantify the strength of the tropopause inversion layer (Birner et al. 2002; Grise et al. 2010), because its spatial variability is much larger than that of N^2.

3. Annual mean

Figure 2 shows the annual climatology of the three CPT properties and their biases from the radiosonde observations (dots in Figs. 2a,b). The annual-mean CPT properties of the radiosonde observation are computed from monthly-mean values. Out of the total 48 months, the stations that have 40 (or more) monthly-mean values available are used for the comparison, and the monthly-mean values are considered only when the number of CPT observations is equal to or greater than 20 for a month. The bias is defined as the difference between the value from radiosonde observation and the value at the nearest grid point obtained from COSMIC observations. It can be seen that, although some sampling errors are possible, the values derived from COSMIC observations are generally in good agreement with those from radiosonde observations. The temperature bias is less than 2 K in the tropics and less than 0.5 K in the deep tropics, and the pressure bias is around 2 hPa. This confirms that temperature profiles derived from GPS radio occultation measurements are reliable in the UTLS (Anthes et al. 2008; He et al. 2009; Kishore et al. 2009).

It is evident from Fig. 2a that annual-mean T-CPT has a significant longitudinal structure with a distinct minimum over the western Pacific and two secondary minima over South America and western Africa. As discussed in the literature (e.g., Highwood and Hoskins 1998; Seidel et al. 2001; Gettelman et al. 2002b; Randel et al. 2003), this zonal asymmetry is associated with localized deep convection (Fig. 2d) and related UTLS processes. As noted by Son et al. (2011), T-CPT fields, however, do not exactly match with OLR fields. For instance, the T-CPT minimum over the WP is located slightly eastward of the corresponding OLR minimum, whereas the minimum over the South America is located slightly westward of the corresponding OLR minimum. This mismatch is apparent in the seasonal-mean field and, as discussed below, this suggests that T-CPT is not solely controlled by deep convection but that other processes such as convectively driven waves or large-scale tropical circulations would also play a role, as discussed by Highwood and Hoskins (1998) and Seidel et al. (2001).

Annual-mean P-CPT, presented in Fig. 2b, shows a different spatial distribution from T-CPT. First, a weak local maximum is observed over Indonesia, where convection is most active. This local structure is, however, not well related to the T-CPT field. Second, no clear longitudinal structure, except over Indonesia, is found in

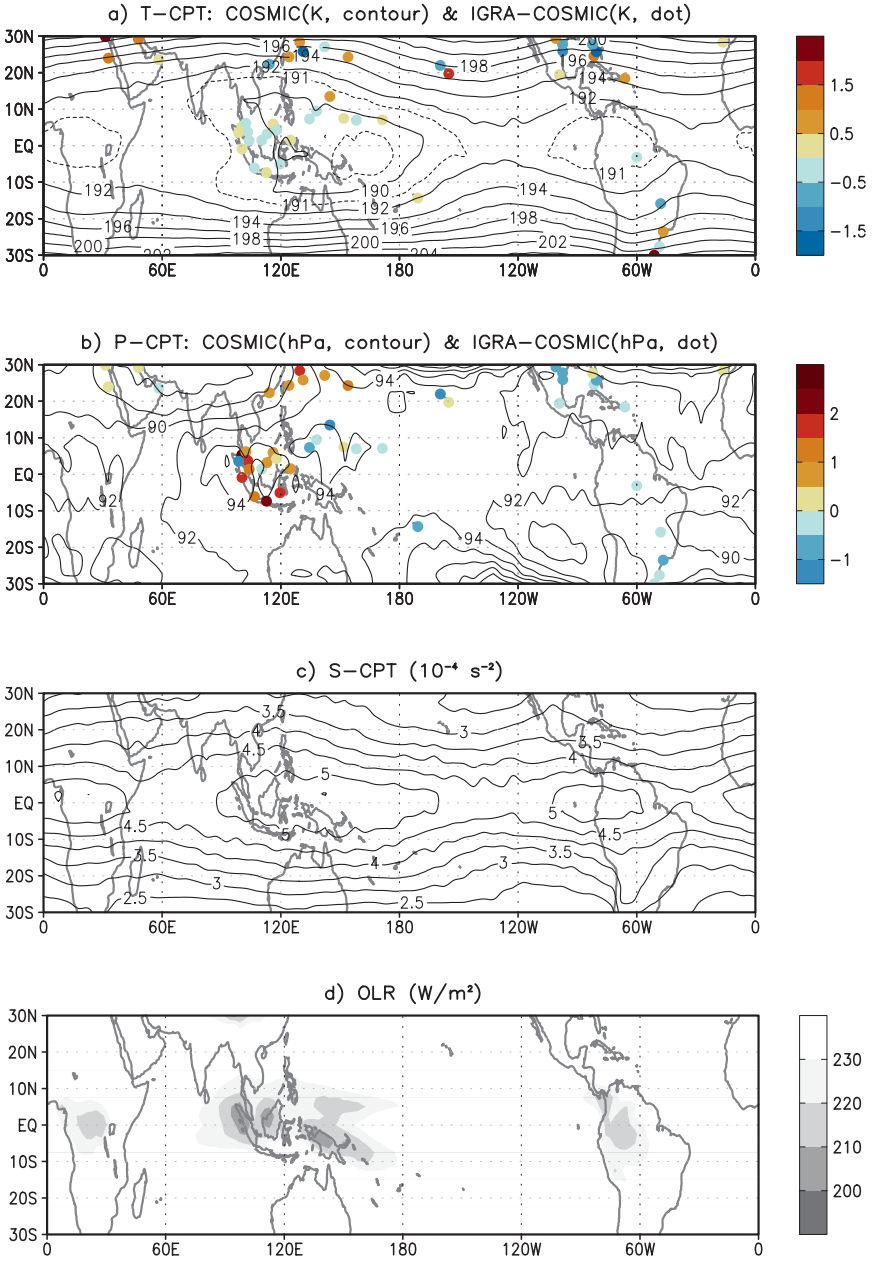

FIG. 2. Annual-mean CPT properties, (a) T-CPT, (b) P-CPT, and (c) S-CPT from COSMIC measurements (contours) and their differences to radiosonde measurements (dots). (d) Annual-mean OLR is also shown. For T-CPT, the 189.5- and 191-K contour lines are shown with the dashed lines.

the deep tropics. In other words, the localized T-CPT minima over the South America and western Africa (Fig. 2a) are not accompanied by localized minima or maxima of P-CPT. Finally, P-CPT is largely homogeneous in the latitudinal direction over 20°S–20°N. Exceptions are found only over the Tibetan Plateau and the South Pacific. It contrasts to latitudinal distribution of T-CPT, which gradually increases with latitude (Figs. 2a).

Figure 2c presents the spatial distribution of S-CPT. The overall structure of S-CPT is qualitatively similar to that of T-CPT, except for its narrow latitudinal extent and small-scale features. This similarity between S-CPT and T-CPT is not surprising, because S-CPT is a function of temperature lapse rate [cf. Eq. (1)]. Cold T-CPT tends to decrease the temperature lapse rate in the lower stratosphere (thus increasing N_+^2) but increases the lapse

rate in the upper troposphere (decreasing N^2_-). This can cause an N^2 difference across the CPT to increase with decreasing T-CPT.

4. Seasonal mean

a. Spatial (latitude–longitude) structure

Figure 3 shows the spatial distribution of CPT properties during boreal winter [December–February (DJF)] and summer [June–August (JJA)]. Consistent with previous studies, it is evident that the CPT is colder, higher (lower in pressure), and sharper during boreal winter than boreal summer, throughout the tropics [e.g., Nishida et al. 2000; Seidel et al. 2001; Randel et al. 2003; Schmidt et al. 2004; Reid and Gage 1981, for lapse-rate tropopause (LRT)]. The seasonal cycle of S-CPT broadly follows that of T-CPT, with an out-of-phase relationship. It is also consistent with the seasonal cycle of the tropopause inversion layer (e.g., Grise et al. 2010).

The structure of T-CPT in DJF much resembles that of the annual-mean T-CPT (Fig. 3a), indicating that the T-CPT climatology is dominated by boreal winter characteristics. As reported in the literature (Gettelman et al. 2002b; Randel et al. 2003), the minima of T-CPT broadly coincide with deep convection, which are presented by minima of OLR. This coincidence can be explained by either radiative cooling by cirrus clouds over the regions of deep convection (Hartmann et al. 2001) or diabatic cooling through convective detrainment (Sherwood et al. 2003; Kuang and Bretherton 2004). The T-CPT minimum locations, however, do not exactly match those of the deep convection. All three localized minima occur right at the equator, north of OLR minima in DJF (Fig. 3a). The same is also true during JJA (Fig. 3d). Although minimum T-CPT is observed in the Indian monsoon region where convection is most active, no secondary minima in T-CPT are found at the eastern Pacific or western Africa, where OLR shows local minima. This result suggests that the formation and maintenance of T-CPT is not solely controlled by deep convection. The equatorial alignment of T-CPT minima could be explained by a planetary-scale wave response to convective heating. Randel et al. (2003) showed that the vertical structure of the near-CPT temperature anomalies over the WP is qualitatively similar to the transient response of equatorial waves to convection. Because these waves are often trapped at the equator, their response appears along the equator, even though convection occurs slightly off the equator. Gettelman and Birner (2007) also indicated that the large-scale response of equatorial waves to convective heating is more important than the details of convection for the climatological structure of the tropical tropopause.

As depicted in the annual average, P-CPT shows a broadly uniform distribution over the tropics in both seasons, except over the South Pacific in DJF and the Tibetan Plateau in JJA. No clear relationship between P-CPT and OLR is found in either season. Again, this indicates that the CPT is not simply controlled by deep convection. The spatial distribution of S-CPT resembles that of T-CPT in both seasons (Figs. 3c,f). It is also similar to that of the tropopause inversion layer reported in Grise et al. (2010). Interestingly, however, maximum S-CPT during DJF is found over South America, where T-CPT is warmer than the WP. This indicates that S-CPT is more sensitive to the temperature lapse rate in the lower stratosphere or upper troposphere than to temperature itself.

b. Meridional structure

The monthly-mean climatology of zonal-mean CPT properties is presented in Figs. 4a–c along with OLR (Fig. 4d). As already shown in Fig. 3, the CPT shows colder T-CPT, lower P-CPT, and sharper S-CPT during boreal winter than during boreal summer, although amplitudes and latitudinal extents differ among CPT properties. Over the equator, the maximum seasonal differences of T-CPT, P-CPT, and S-CPT are approximately 5 K (~3%), 14 hPa (~15%), and 10^{-4} s^{-2} (~20%), respectively. The zonal-mean P-CPT is largely homogeneous over the tropics, except in the Northern Hemispheric subtropics during boreal winter. It contrasts with the other properties, which show noticeable meridional gradient. It is also noteworthy that S-CPT shows secondary maxima on April, and its latitudinal extent and seasonal cycle are limited in the deep tropics, whereas other properties show a significant seasonal cycle in the whole tropics.

It is evident from Fig. 4 that minimum zonal-mean T-CPT and maximum zonal-mean S-CPT are always located over the equator. No latitudinal migration is found in these properties in stark contrast to zonal-mean OLR, which exhibits significant latitudinal displacement with season. More importantly, the seasonal cycle of CPT properties does not match well with tropospheric temperature (see Fig. 6f of Son et al. 2011). These results provide evidence that the seasonal cycle of CPT properties is not controlled by convection, although spatial distribution, especially the seasonal minima of T-CPT, is to some degree affected by deep convection (Highwood and Hoskins 1998; Seidel et al. 2001).

To further examine the relationship between tropical deep convection and CPT properties, monthly-mean climatologies of T-CPT, P-CPT, and OLR are analyzed over the two regions: the western Pacific over 10°S–5°N and 100°E–180° and the Indian summer monsoon region over 5°–20°N and 60°–140°E (Fig. 5). These two regions

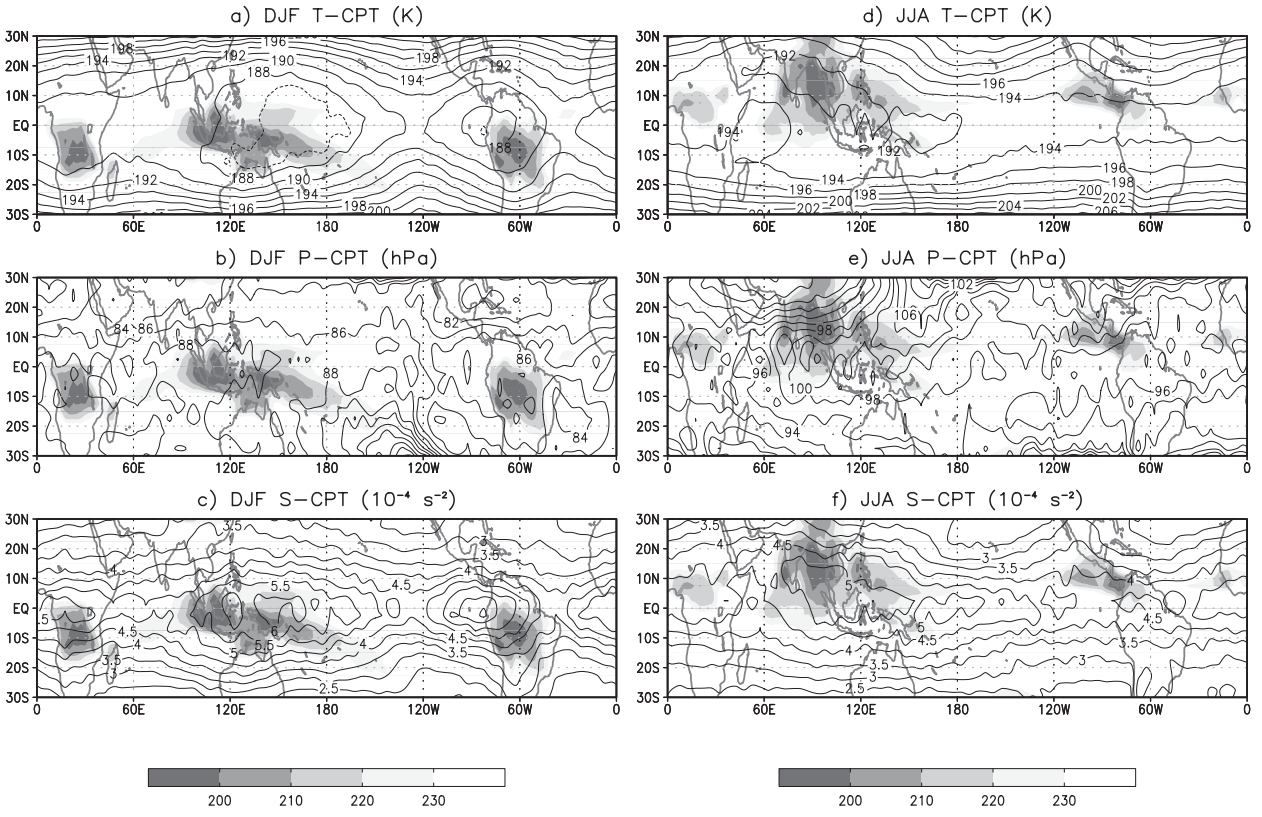

FIG. 3. Seasonal-mean (top to bottom) T-, P-, and S-CPT properties in (a)–(c) DJF and (d)–(f) JJA. Superimposed shading denotes OLR for each season. For T-CPT, the 187-K contour line is shown by the dashed line.

are chosen as they are the regions of minimum T-CPT during DJF and JJA (Figs. 3a,d). Although seasonal cycles of OLR in these two regions are almost opposite (Fig. 5c), both T-CPT and P-CPT exhibit essentially the same seasonal cycle. This suggests that the seasonal cycle of CPT properties is likely modulated by large-scale processes rather than small-scale local processes. In fact, it is known that seasonality in the tropical lower stratosphere is largely controlled by upwelling driven by wave forcings in the extratropical lower stratosphere (Yulaeva et al. 1994; Holton et al. 1995). The upwelling is stronger during DJF than during JJA, resulting in colder T-CPT in DJF through adiabatic cooling (Seidel et al. 2001; Gettelman et al. 2002a; Fueglistaler et al. 2009).

Figure 6 presents a signature of the upwelling using monthly-mean zonal-mean tropical temperature anomalies. Here anomaly is defined by deviation from the 4-yr mean value. The temperature anomalies show a clear seasonal cycle along with interannual variability as documented in previous studies (e.g., Randel et al. 2003; Schmidt et al. 2004; Fueglistaler et al. 2009). The largest amplitude of temperature anomalies is found just above the CPT, between the CPT and 70 hPa. This feature could be explained by the relatively long radiative relaxation time scale in the region, as shown in Randel et al. (2002). However, it could also be caused by tropical upwelling in the lower stratosphere, which peaks near the tropopause. Fueglistaler et al. (2009) showed that the clear-sky radiative heating rate exhibits a localized maximum in this region during DJF. This suggests that there should be a physical or dynamical cooling to balance this radiative heating. In fact, the vertical structure of temperature anomaly is consistent with that of upwelling (adiabatic cooling) estimated from tracer transport (Mote and Dunkerton 1998; Boehm and Lee 2003). Although detailed dynamical mechanisms of the near-CPT temperature anomaly are beyond the scope of the present study, the temperature anomalies are likely caused not only by the Brewer–Dobson circulation (Yulaeva et al. 1994) but also by the near-CPT upwelling driven by tropospheric eddy momentum fluxes (Boehm and Lee 2003; Kerr-Munslow and Norton 2006; Norton 2006; Randel et al. 2008). Kerr-Munslow and Norton (2006) and Norton (2006) proposed that planetary-scale waves, largely forced by tropical convection, can influence the upwelling near the CPT. Boehm and Lee (2003) and Randel et al. (2008) further suggested that

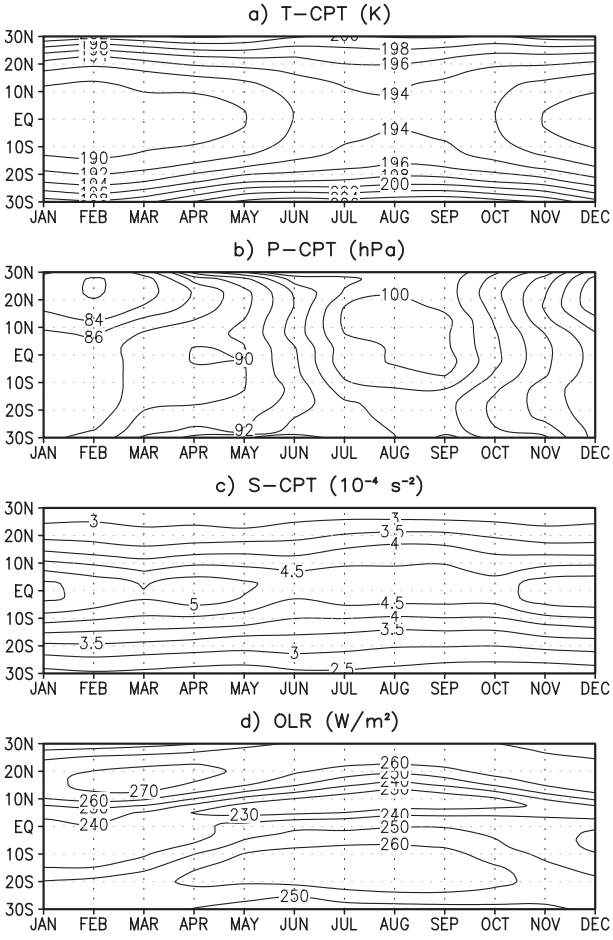

FIG. 4. The 4-yr climatologies of monthly-mean zonal-mean (a) T-CPT, (b) P-CPT, (c) S-CPT, and (d) OLR as a function of latitude.

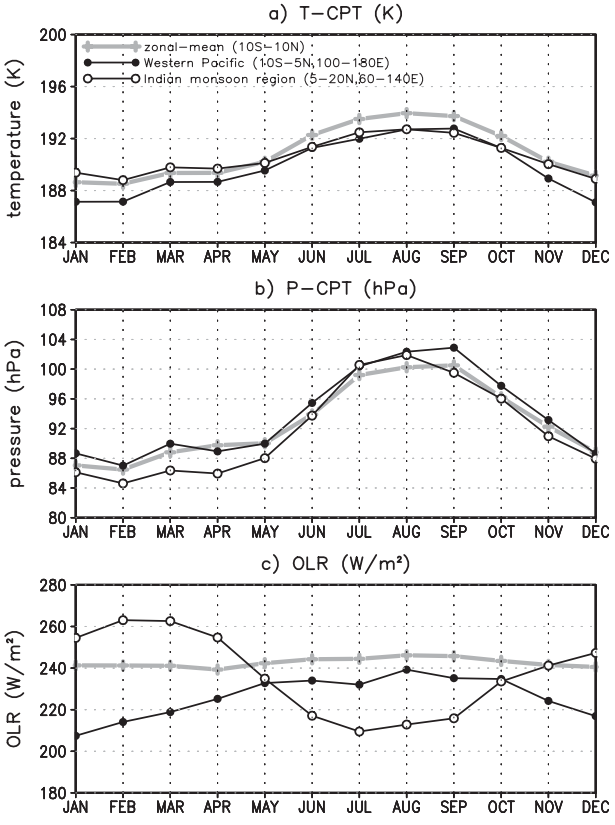

FIG. 5. The 4-yr climatologies of monthly-mean (a) T-CPT, (b) P-CPT, and (c) OLR averaged over the deep tropics (10°S–10°N, 180°–180°), WP (10°S–5°N, 100°E–180°), and Indian monsoon region (5°–20°N, 60°–140°E).

equatorial upwelling is at least partly affected by horizontal convergence of eddy momentum flux near the tropical tropopause. They particularly showed that eddy momentum flux convergence near the tropical tropopause is stronger in boreal winter than in summer.

c. *Zonal structure*

It is known that the horizontal distribution and seasonal cycle of T-CPT are not homogeneous in longitude (Highwood and Hoskins 1998; Randel et al. 2003; Fueglistaler et al. 2009). Figure 7 presents the longitudinal structure of T-CPT and P-CPT over the deep tropics and their time evolution. S-CPT is not shown because it is qualitatively similar to T-CPT. It can be seen that T-CPT has distinct warm regions around 120°–140°W and 30°W during boreal winter (see also Fig. 3a). Although interannual variability is not negligible, T-CPT in these two regions is generally warmer than in other regions during boreal winter, resulting in a weak seasonal cycle of T-CPT there (Fig. 7a, bottom). In contrast to T-CPT and as discussed in the previous section, longitudinal dependency is essentially absent in P-CPT (Fig. 7b).

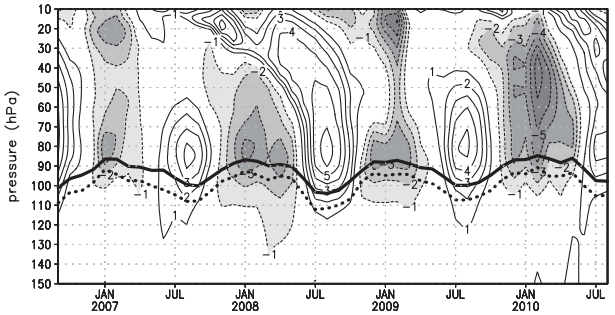

FIG. 6. Monthly-mean zonal-mean temperature anomalies averaged over the deep tropics (10°S–10°N, 180°–180°). Anomaly is defined by deviation from long-term mean (September 2006–August 2010). Contour interval is 1 K, and the 0 line is omitted. P-CPT (thick solid line) and P-LRT (thick dotted line) are also shown for reference.

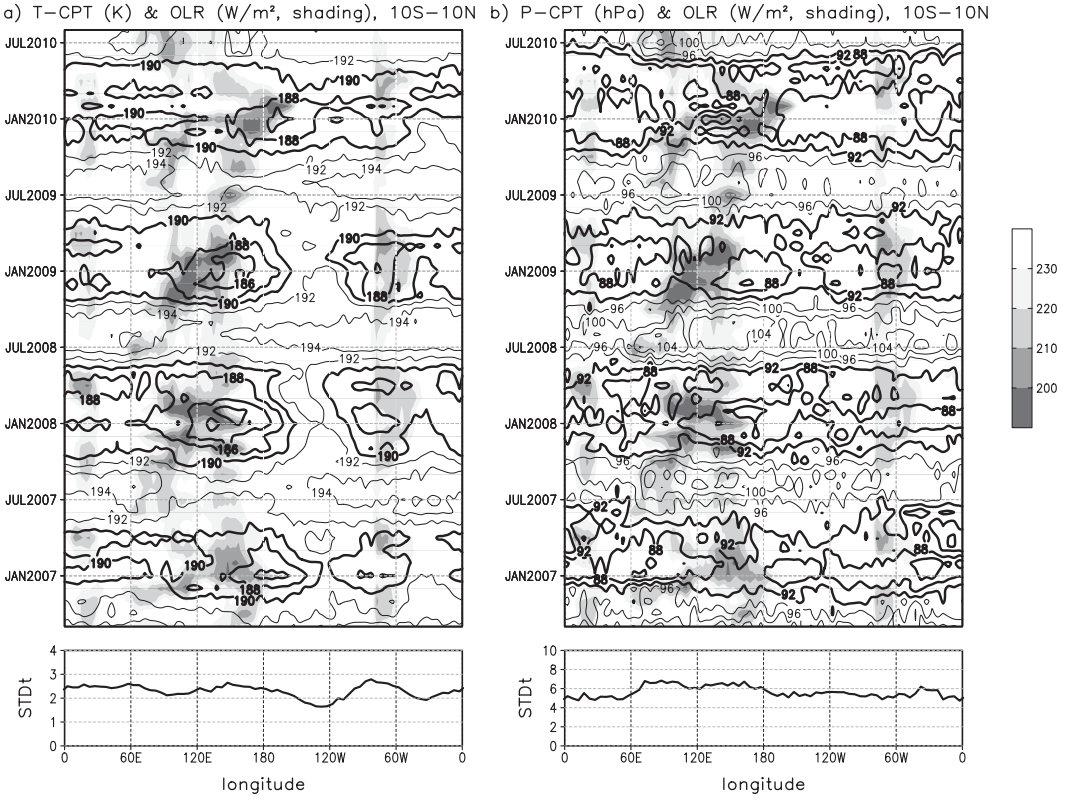

FIG. 7. Hovmöller diagram of monthly-mean (a) T-CPT and (b) P-CPT averaged over 10°S–10°N. Contour intervals are 2 K and 4 hPa, respectively and values ≤ 190 K or 90 hPa are indicated with thick contour lines. In both panels, OLR averaged over 10°S–10°N is superimposed with shading. Standard deviation of each property, quantifying seasonal and interannual variabilities, is also shown in the bottom panel.

To better understand the difference between T-CPT and P-CPT in longitudinal structure, DJF-mean temperature profiles are compared over the regions of strong (140°–160°E) and weak (120°–140°W) seasonalities of T-CPT (Fig. 8a). The temperature profiles show significant difference at the CPT level with almost no difference above ~60 hPa. This suggests that the T-CPT difference between the two regions is not likely originated from the stratosphere. As expected from Fig. 7b, no significant difference is, however, found in P-CPT; P-CPT values in the two regions are indistinguishable from the zonal-mean value. It turns out that the CPT is too sharp to be modified by temperature perturbations in the vicinity. Figure 8b presents the temperature profiles on the tropopause-relative vertical coordinate, where individual temperature profiles are averaged with respect to the CPT as in Birner (2006). The temperature minimum at the CPT is very sharp. As a result, local temperature changes in the UTLS can hardly change the CPT level. This also explains the zonally uniform structure of P-CPT found in Figs. 3b,e. As discussed in Shepherd (2002), a thermal forcing that has a deep vertical structure (e.g., adiabatic cooling due to Brewer–Dobson circulation) can effectively modify P-CPT.

Returning to the longitudinal structure of T-CPT shown in Fig. 7, relatively warm T-CPT over 120°–140°W and 30°W could be attributed to weak convection (shading) there. It is, however, questionable whether these result directly from tropical convection or other related processes. In fact, warm T-CPT over 120°–140°W can be related to the Walker circulation, whose downward branch is located over the mideastern Pacific (Zhou et al. 2001b; Fueglistaler et al. 2009). Figure 9a presents vertical velocity at 100 hPa from ERA-Interim. Although caution is needed here, because vertical velocity of reanalysis is poorly constrained in data assimilation, the upward motion (adiabatic cooling) over the western Pacific and downward motion (adiabatic warming) over the mideastern Pacific match broadly with the relatively cold and warm T-CPT, respectively. This suggests that the longitudinal structure of T-CPT is likely controlled by deep convection and the related large-scale circulation in the tropical troposphere. It is

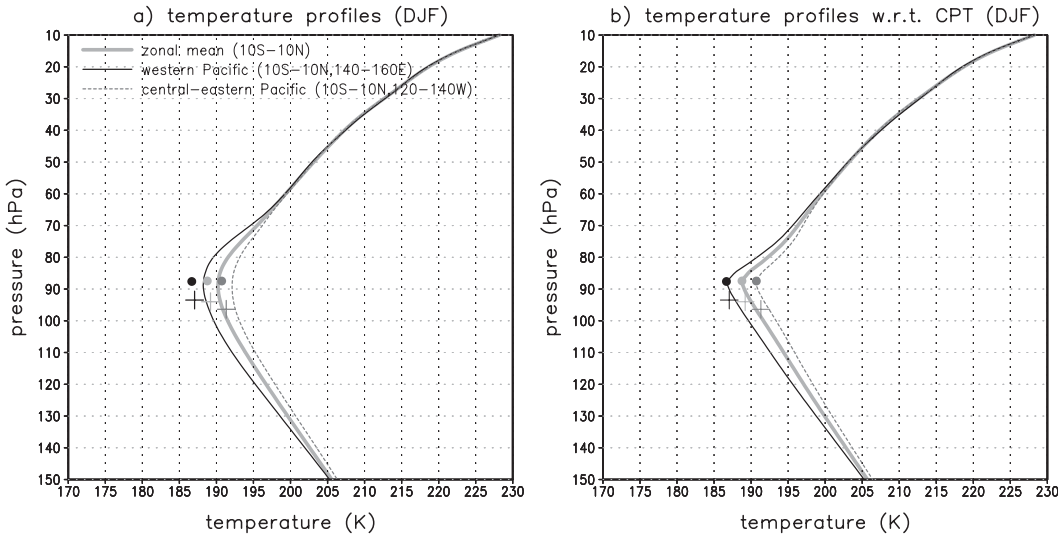

FIG. 8. DJF-mean temperature profiles averaged over the deep tropics (10°S–10°N, 180°–180°) and western (10°S–10°N, 140°–160°E) and central Pacific (10°S–10°N, 120°–140°W) regions (a) on the conventional pressure coordinate and (b) on the tropopause-relative pressure coordinate. Dots and crosses denote location of the CPT and the LRT, respectively. On the tropopause-relative pressure coordinate, individual temperature profiles are averaged with respect to the CPT by moving each CPT level to the climatological CPT level. Hence, pressure level denotes relative pressure distance from CPT, instead of actual pressure level. Note in (a) that the CPT and LRT are not located on the profile because individual temperature profiles are smoothed through time and area average.

worth noting that the relatively zonal structure in T-CPT during the boreal winter (DJF) of 2009/2010 could be associated with the 2010 El Niño event, because El Niño can flatten the thermal structure of the CPT by disturbing the Walker circulation.

The above result, however, does not exclude the influence of other possibilities such as circulations driven by tropical or extratropical eddies. Figure 9b presents monthly-mean zonal wind at 100 hPa. During boreal winter, regions of relatively warm T-CPT are very well matched with those of westerly winds. Longitudinal width of the warm T-CPT region is also highly coherent with that of westerlies on seasonal and interannual time scales. Although not shown, a similar relation is also found on intraseasonal time scale, indicating that relatively warm T-CPT over the two regions, the mideastern Pacific and Atlantic Oceans, is strongly correlated with the equatorial westerlies in the UTLS. This result hints at the possible role of tropical or extratropical eddies that deposit westerly momentum in the region. In particular, tropical stationary eddies associated with deep convection are known to deposit westerly momentum in the deep tropics (e.g., Lee 1999; Dima et al. 2005). Although this westerly momentum is balanced by easterly momentum advection resulting from cross-equatorial mean meridional circulation in the zonal-mean perspective (Dima et al. 2005), longitudinal imbalance of momentum can exist because meridional circulation varies with longitude. Regardless of dynamical mechanisms, a local westerly momentum source needs to be balanced by the Coriolis torque of equatorward flow and could induce local downwelling by mass continuity (Haynes et al. 1991). The opposite can also occur (i.e., easterly momentum and upwelling; e.g., Randel et al. 2008). Although the eddy-driven vertical motion and the convectively driven large-scale circulation may not be separable, the coherence between the warm CPT and the westerly wind suggests that tropical or extratropical eddies may play an important role in setting the longitudinal structure of T-CPT. Further study is needed.

5. Intraseasonal variability

Because the intraseasonal variability of T-CPT is directly related with various physical processes in the tropical UTLS, such as the formation of cirrus cloud (Eguchi and Shiotani 2004) and cross-tropopause transport of water vapor (Mote et al. 2000; Eguchi and Shiotani 2004), it has been extensively examined in the recent decade (e.g., Kiladis et al. 2001; Zhou and Holton 2002; Randel et al. 2003; Randel and Wu 2005; Suzuki and Shiotani 2008). Although it is well established that short-term variability of the CPT properties is largely controlled by deep convection and the resulting tropical waves in the UTLS (e.g., Zhou and Holton 2002; Randel and Wu 2005; Son and Lee 2007), current understanding

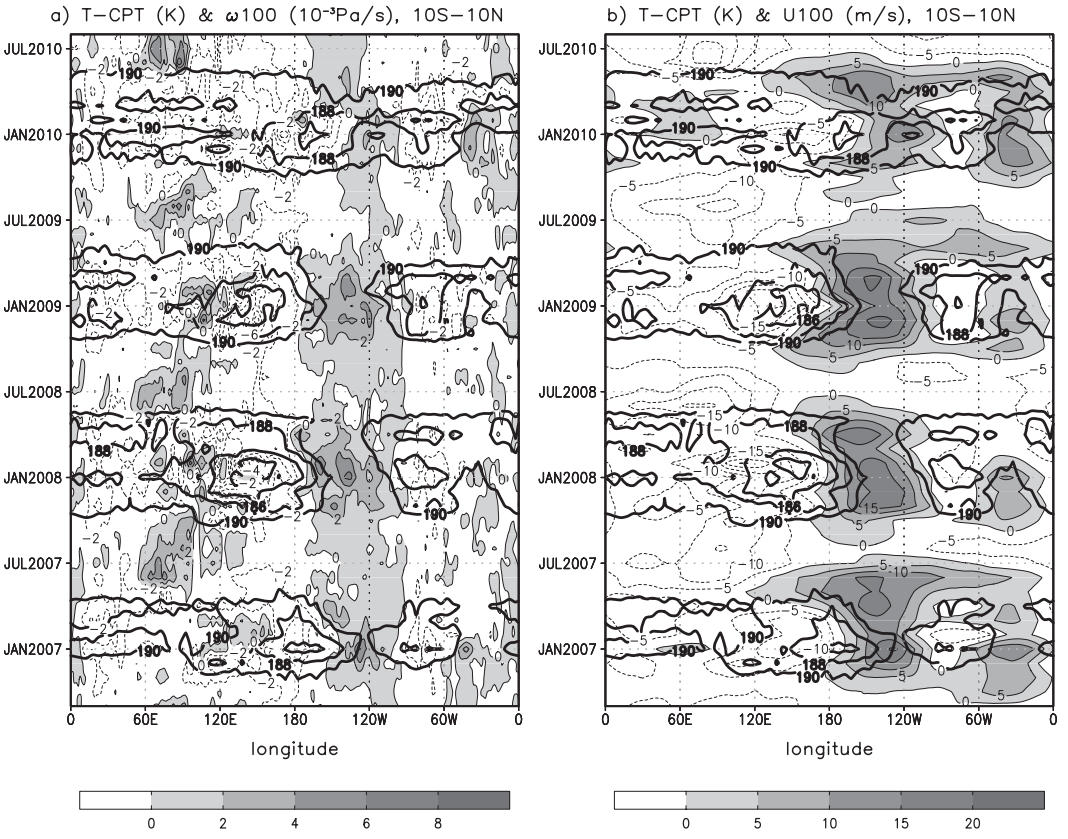

FIG. 9. Hovmöller diagram of monthly-mean (a) 100-hPa vertical velocity (omega) and (b) 100-hPa zonal wind; both are averaged over 10°S–10°N (shading and thin contour) and superimposed on the monthly-mean T-CPT (thick contour). Vertical velocity and zonal wind are from ERA-Interim. Contour and shading intervals are 2 K for T-CPT, 2×10^{-3} Pa s^{-1} for omega, and 5 m s^{-1} for zonal wind. Only T-CPT values ≤ 190 K are presented. Positive values are shaded for vertical velocity and zonal wind.

is mostly based on reanalysis data at a fixed or interpolated level. In this section, the intraseasonal variability of the CPT is revisited with high-resolution observations. The variability is first examined by means of the standard deviation σ, as in Son et al. (2011). This is computed by subtracting a monthly mean from instantaneous values and then taking standard deviation of the anomalies at a given month. The power spectra and space–time-filtered data are then examined by applying wavenumber–frequency analysis (Wheeler and Kiladis 1999).

a. Spatiotemporal structure

Figure 10 shows the σ of three CPT properties and their seasonal dependencies. Both σ of T-CPT ($\sigma_{\text{T-CPT}}$) and P-CPT ($\sigma_{\text{P-CPT}}$) exhibit a relatively uniform pattern in longitude and latitude within 20°S–20°N. They then sharply increase in the subtropics across the subtropical jet. Somewhat surprisingly, no coherence is observed between $\sigma_{\text{T-CPT}}$ (and also $\sigma_{\text{P-CPT}}$) and deep convection even in DJF; $\sigma_{\text{T-CPT}}$ and $\sigma_{\text{P-CPT}}$ are not spatially correlated with σ_{OLR}. Furthermore, no pronounced seasonal dependence is found in the spatial structure and magnitude of $\sigma_{\text{T-CPT}}$ and $\sigma_{\text{P-CPT}}$, as shown in Figs. 10 and 11. These are in stark contrast with climatological CPT properties, which show significant spatial structure and seasonality (Figs. 3, 4), suggesting that the driving mechanisms of the intraseasonal variability of the CPT is different from that of climatology. It is worthwhile to note that, although qualitatively similar results are also found in the LRT (Schmidt et al. 2005; Son et al. 2011), $\sigma_{\text{P-CPT}}$ is somewhat weaker than $\sigma_{\text{P-LRT}}$, and more importantly $\sigma_{\text{P-CPT}}$ does not show localized maximum over the Tibetan Plateau in boreal summer in contrast to $\sigma_{\text{P-LRT}}$ (see Figs. 7, 9 of Son et al. 2011). This indicates that the CPT is generally well defined.

It is evident from Figs. 10c,f that the $\sigma_{\text{S-CPT}}$ has a different spatial distribution from $\sigma_{\text{T-CPT}}$, unlike their climatologies. Especially during boreal winter $\sigma_{\text{S-CPT}}$ shows three local maxima along the equator, where $\sigma_{\text{T-CPT}}$ and $\sigma_{\text{P-CPT}}$ are at a minimum. In addition, $\sigma_{\text{S-CPT}}$ shows a nonnegligible seasonal cycle in the deep tropics: it

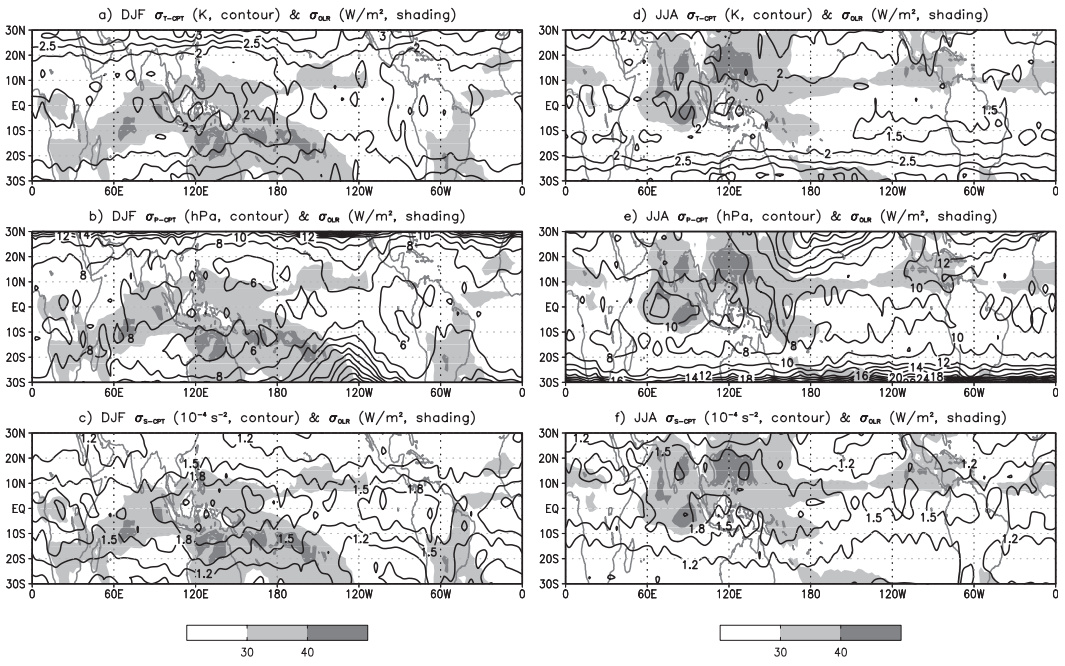

FIG. 10. As in Fig. 2, but for intraseasonal variability that is defined by the standard deviation from monthly mean. Contour intervals are 0.5 K for σ_{T-CPT}, 2 hPa for σ_{P-CPT}, and 0.3 s^{-2} for σ_{S-CPT}. Shading is σ_{OLR}.

is stronger during boreal winter than during the summer (see also Fig. 11c). This spatial pattern and seasonal dependency of $\sigma_{S\text{-}CPT}$ resemble those of climatological S-CPT (cf. Figs. 3, 10; also cf. Figs. 4c, 11c), suggesting that the short-term variability and long-term mean of S-CPT may be controlled by the same physical process(es).

The above findings, especially minimum $\sigma_{T\text{-}CPT}$ and $\sigma_{P\text{-}CPT}$ but maximum $\sigma_{S\text{-}CPT}$ in the deep tropics, might be puzzling. The former, however, can be understood by the fact that top of tropical convection is typically lower than the CPT level (Gettelman et al. 2002b). The latter can be explained by the fact that S-CPT is not only a function of temperature but also a function of the temperature lapse rate. Although not shown here, $\sigma_{S\text{-}CPT}$ is to a large degree determined by the short-term fluctuation of the temperature lapse rate above the CPT. As discussed below, lapse rate fluctuation is highly associated with convectively driven equatorial waves, which propagate in the zonal and vertical directions. For instance, vertically tilted equatorial Kelvin waves (e.g., Fig. 6 of Wheeler et al. 2000) can significantly modify the temperature lapse rate in the UTLS. We note here that, although the magnitude of $\sigma_{T\text{-}CPT}$ is generally small and homogeneous over 20°S–20°N, it is slightly larger at the equator than off the equator near 10°N and 10°S (Figs. 10a,d). This weak equatorial maximum is found in most seasons (Fig. 11a) and is also likely associated with the equatorially trapped waves.

The weak relationship between $\sigma_{T\text{-}CPT}$ and σ_{OLR} (shown in Figs. 10, 11), however, should not be interpreted as a lack of convective influence on the CPT. Figure 12 shows a Hovmöller diagram of the 3-day running mean T-CPT and OLR averaged over 10°S–10°N. Here, the 3-day running mean is applied to increase sample size and to reduce high-frequency noise. Only one year, from July 2007 to June 2008, is presented as an example. It can be seen that, although T-CPT fluctuates almost randomly in time, an organized eastward propagation is evident in the western Pacific during boreal winter; relatively cold T-CPT propagates slowly from 70°E to the date line from December 2007 to January 2008. This organized propagation is highly collocated with OLR anomaly, which represents MJO convection during the time. This result suggests that the intraseasonal variability of T-CPT is at least locally associated with deep convection, as shown in Zhou and Holton (2002) from reanalysis data.

b. Wavenumber–frequency spectrum

To examine more detailed variability of the CPT, a power spectrum analysis is performed for CPT properties and OLR as in Wheeler and Kiladis (1999). The latitudinal integration over 10°S–10°N (only symmetric part) and 3-day running mean are first applied as in Fig. 12. Anomalies are then defined by removing the first 12 harmonics from the 4-yr time series at each longitudinal

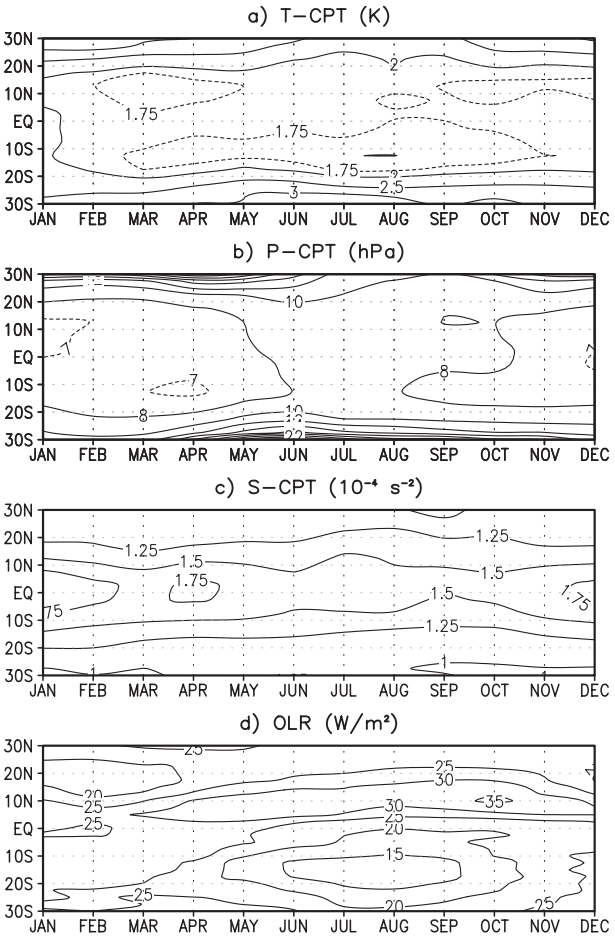

FIG. 11. As in Fig. 4, but for intraseasonal variability.

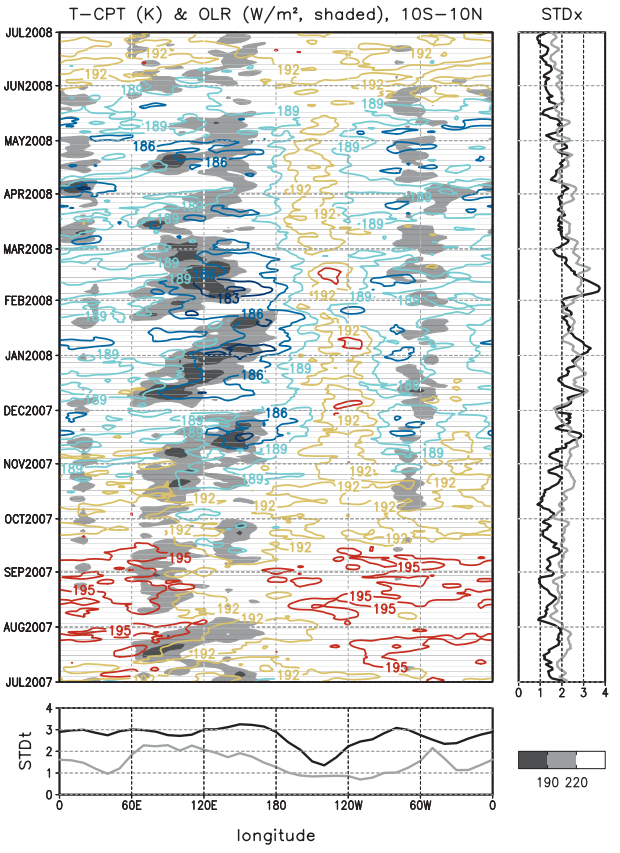

FIG. 12. Hovmöller diagram of the T-CPT (contours) and OLR (shading) averaged over 10°S–10°N from July 2007 to June 2008. High-frequency variability is slightly dampened by applying a 3-day running mean. Standard deviations of the T-CPT (black line) and OLR (gray line) (bottom) in time and (right) in longitude are also shown. The standard deviations of OLR are scaled with a factor of 0.1 for graphical convenience.

grid point; the 12th harmonic component has a period of ~122 days. By doing this, we remove seasonal cycle and interannual variability and isolate only short-term variability. These anomalies are subject to the spectral analysis. For the spectral analysis, a 96-day time window with 60-day overlapping is used, and with this 38 samples are obtained during the analysis period. The results are shown for T-CPT and OLR in Fig. 13. P-CPT and S-CPT spectra are not shown because they are qualitatively similar to T-CPT.

Figure 13 shows that intraseasonal variability of the CPT is largely due to equatorial Kelvin waves and MJO convection. Although overall power spectrum of T-CPT is qualitatively similar to that of OLR, it is important to note that they do not exactly match in both high-frequency (4–30 days) and low-frequency (30–96 days) bands. In the high frequency, the maximum power of T-CPT anomalies is found at the Kelvin wave band at an equivalent depth of 50–240 m, whereas that of the OLR anomalies is found at an equivalent depth of ~50 m. In other words, the Kelvin wave components of the T-CPT anomalies propagate faster and are not fully coupled with convection. Those fast-moving anomalies are likely associated with free (internal) Kevin waves. Although free Kelvin waves might initially be excited by deep convection, they typically travel faster than convectively coupled ones (Zhou and Holton 2002). In the low frequency, a maximum power of T-CPT appears in response to the MJO convection. However, it is found at zonal wavenumber (k) three, which is larger than that of OLR (the maximum power of OLR spectrum is found at $k = 1$). This result does not indicate weak (or no) coupling between T-CPT and OLR. The coherence between the T-CPT and OLR spectra (Fig. 13c) shows that strong coherences exist at $k = 1$ of the MJO band and at $k = 2$ of the Kelvin wave band. The difference in zonal wavenumber results from the fact that T-CPT anomalies have a longer memory than OLR anomalies. As shown in MJO-filtered anomalies (Fig. 14a), the T-CPT anomaly

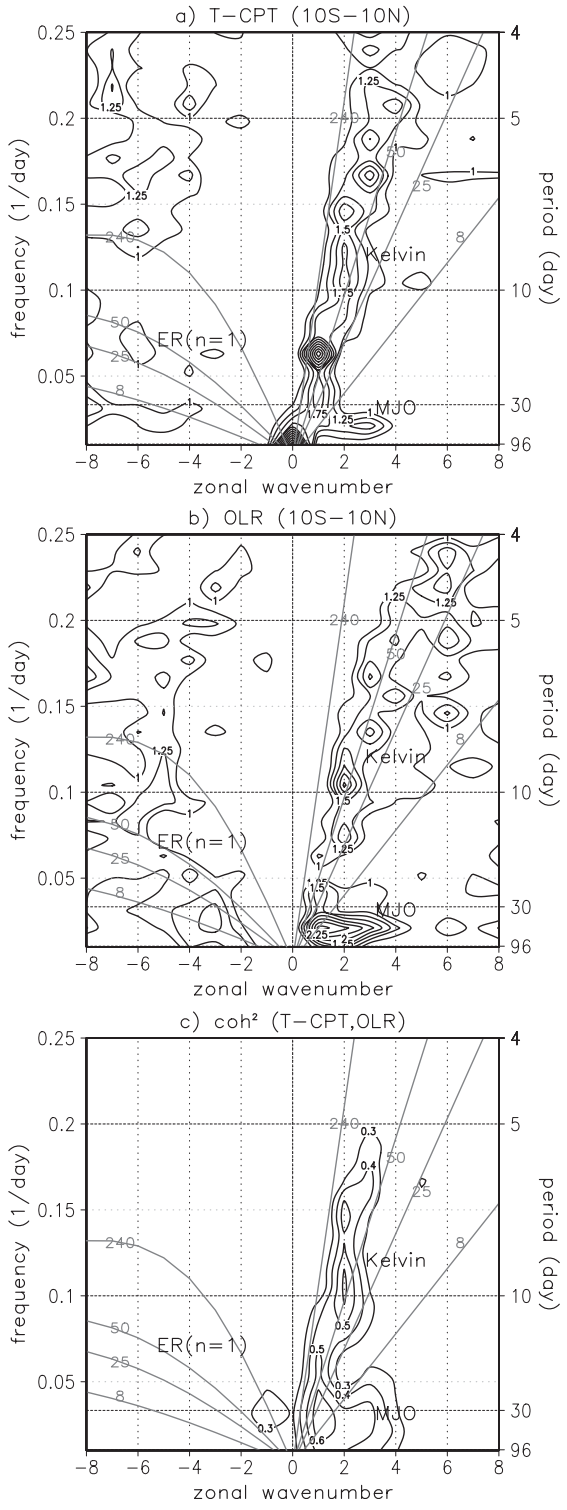

FIG. 13. Wavenumber–frequency power spectra of (a) T-CPT and (b) OLR averaged over 10°S–10°N and (c) their spectral coherence (coherence square). Before performing spectral analysis, data are slightly smoothed by applying a 3-day running mean. Interannual variability and seasonal cycle are also removed by subtracting the first 12 harmonics from the 4-yr-long data.

associated with a given MJO event lasts longer than the corresponding OLR anomaly and propagates to the eastern Pacific, whereas the OLR anomaly dissipates near the date line. This anomaly and the new T-CPT anomaly excited by a new MJO event generate a larger wavenumber.

The temporal evolution of T-CPT and OLR is further analyzed by applying Kelvin wave and MJO filters. Figure 14 presents the MJO and Kelvin wave components of Fig. 12. The MJO component is obtained by taking the variability at k = 1–5 and periods of 30–96 days, and the Kelvin wave component is obtained by taking anomalies at k = 1–9, periods of 4–30 days, and equivalent depths of 8–240 m. These filters are essentially identical to those used in Wheeler and Kiladis (1999), except a small difference in wavenumber and equivalent depth. The MJO-filtered T-CPT anomalies are highly coherent with OLR anomalies (Fig. 14a). As documented in Zhou and Holton (2002), the cold T-CPT anomaly is generally located on the east side of the minimum OLR anomaly, leading a quarter of the wavelength, ~30° in longitude (see also Fig. 15a). This phase shift results from the fact that the temperature perturbation driven by MJO convection tilts eastward with height, as shown in Fig. 16a. Because the top of the convection [~(150–200) hPa] is generally below the CPT [~(90–100) hPa], the temperature anomaly associated with MJO convection appears on the east side of the convection center, at the CPT level.

The relationship between the MJO convection and T-CPT anomalies is summarized in Fig. 15a with a composite map. It is obtained by averaging MJO-filtered T-CPT anomalies for 18 MJO cases during extended winter, October–March (ONDJFM), when MJO convection is active (Fig. 14a, right). These anomalies are selected when MJO-filtered OLR anomalies are minimum at 110°E, where they show maximum temporal variability (see Fig. 14b, bottom). The T-CPT anomalies near the OLR anomaly are very robust and propagate eastward along with eastward movement of MJO convection. Although not shown, similar coupling between T-CPT and OLR anomalies is also found in boreal summer.

Figure 14b presents the Kelvin wave–filtered T-CPT and OLR anomalies. Unlike the MJO-filtered anomalies, no geographical preference is observed for Kelvin wave activities, although a weak maximum is found at 50°E (see the bottom panel). Also, no seasonal dependency is found (see the right panel). Figure 15b further shows a composite map of T-CPT anomalies for 91 convection events during ONDJFM. A reference longitude is set to 30°E, where Kelvin wave–filtered OLR anomalies show maximum temporal variability. It is found that the convectively coupled T-CPT anomalies

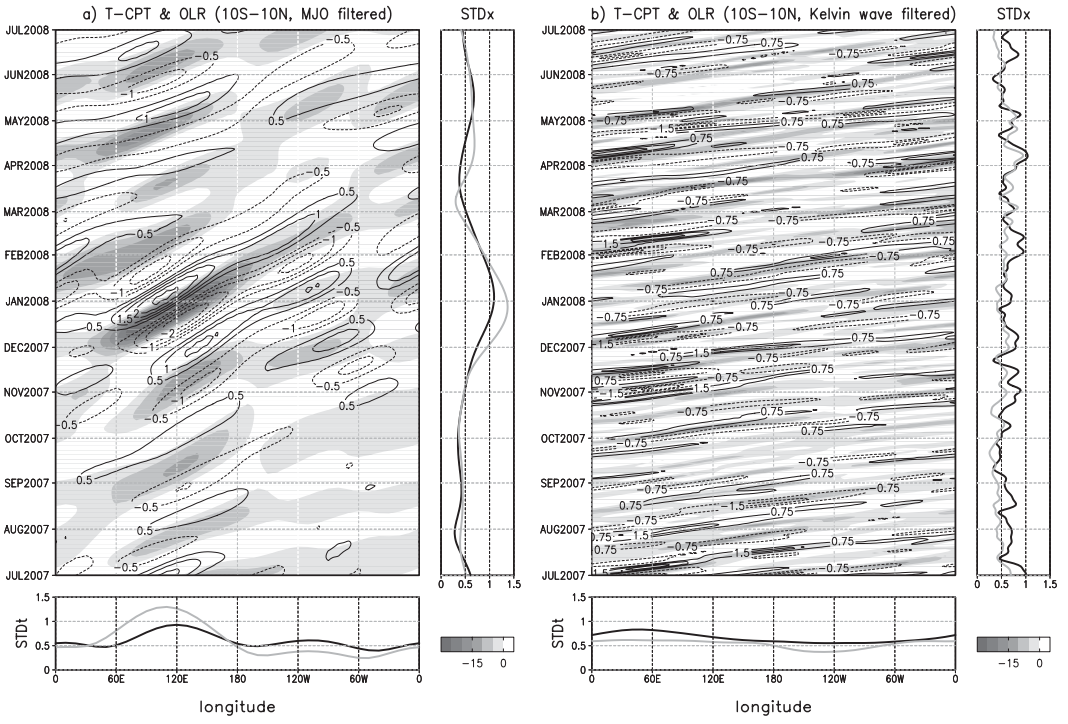

FIG. 14. As in Fig. 12, but for (a) MJO and (b) Kelvin wave bands. Contour intervals are 0.5 K for the MJO band and 0.75 K for the Kelvin wave band.

appear only near the OLR anomaly. From Fig. 14b, it is also found that, although not statistically significant, eastward-propagating T-CPT anomalies are present almost everywhere, even without OLR anomalies. In fact, the coupling itself is not strong. The maximum lag-correlation coefficient between the T-CPT and OLR anomalies is only ~0.5, which is much smaller than the one in the MJO band (~0.9). This provides evidence that

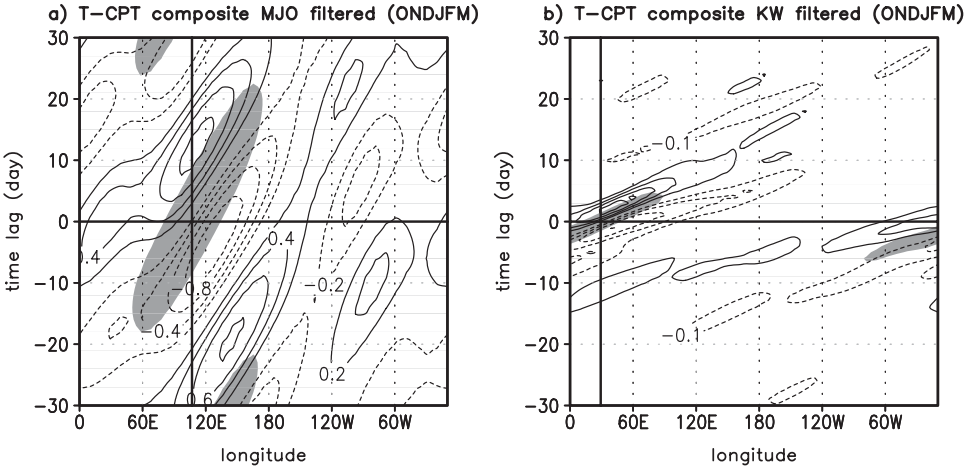

FIG. 15. Composite of T-CPT anomalies averaged over 10°S–10°N for (a) MJO and (b) Kelvin wave bands during extended boreal winter (ONDJFM). Contour intervals are 0.2 and 0.1 K, respectively. The 99% confidence levels are approximately ±0.4 and ±0.2 K, respectively. Shadings denotes composites OLR anomaly for each band. Only OLR anomalies ≤ −4 and −2 W m^{-2} (approximately 99% confidence level) are shaded for MJO and Kelvin wave bands, respectively. Reference longitudes of OLR anomalies (110°E for the MJO component and 30°E for Kelvin wave component) are indicated with vertical lines.

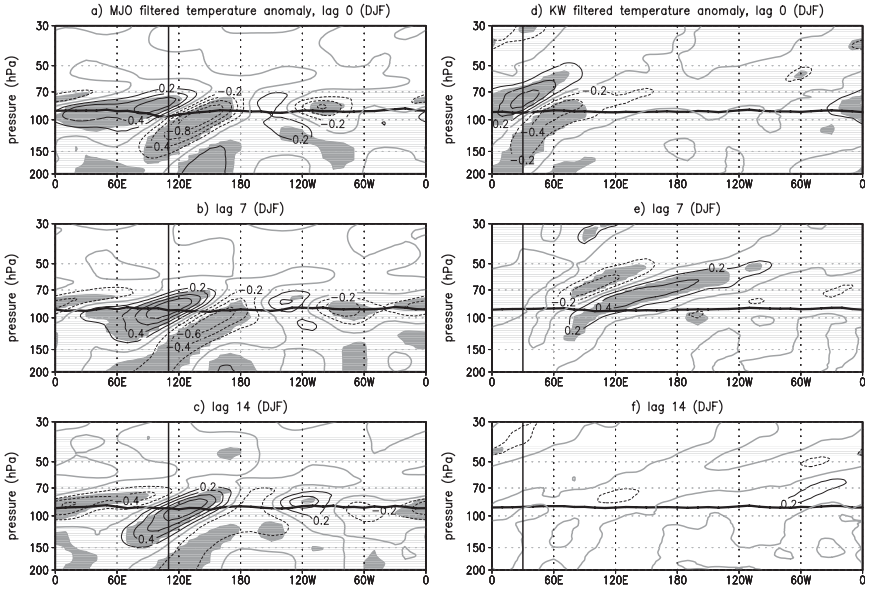

FIG. 16. Composite temperature anomalies averaged over 10°S–10°N for (a) MJO and (b) Kelvin wave band during ONDJFM as a function of longitude and pressure. Shading denotes 99% confidence level. Reference longitudes of OLR anomalies are indicated with vertical lines. Thick horizontal lines denote the location of the CPT.

the Kelvin wave components of T-CPT anomalies are not fully coupled with deep convection. It also explains why $\sigma_{\text{T-CPT}}$ (Figs. 10a,d) shows only weak zonal structure.

The different characteristics of $\sigma_{\text{S-CPT}}$, which are discussed above, are likely associated with the vertical structure of equatorial waves. Figure 16 presents composite temperature anomalies in the deep tropics as a function of longitude and pressure. The anomalies are obtained as in Fig. 15 and only lags of 0, 7, and 14 days are shown. An eastward vertical tilting is evident in both MJO and the Kelvin wave–filtered anomaly as in Wheeler et al. (2000) and Randel et al. (2003). The associated dipole temperature anomalies near the CPT, warm in the lower stratosphere and cold in the upper troposphere, can effectively modify the temperature lapse rate in the UTLS. This results in significant fluctuations of S-CPT at the equator, especially over the active convective regions.

6. Summary and discussion

Finescale structure of the cold-point tropopause (CPT) and its variability is examined in this study using COSMIC GPS radio occultation measurements, which provide accurate temperature profiles in the UTLS with relatively high vertical and medium horizontal (~500 km) resolutions. Overall results are in good agreement with previous studies, which are mostly based on radiosonde observations, reanalysis, and relatively coarse-resolution GPS radio occultation data (e.g., Randel et al. 2000; Nishida et al. 2000; Seidel et al. 2001; Gettelman et al. 2002b; Zhou and Holton 2002; Randel et al. 2003; Schmidt et al. 2004; Randel and Wu 2005; Kishore et al. 2006; Fueglistaler et al. 2009). More quantitative and comprehensive results are, however, presented in this study for three CPT properties: CPT temperature (T-CPT), pressure (P-CPT), and sharpness (S-CPT). In particular, intraseasonal variability of each CPT property, which has not been well documented using high-resolution observations, sheds a new light on CPT understanding.

The annual-mean T-CPT shows a significant longitudinal structure with pronounced minima on the equatorial western Pacific, South America, and western Africa. These minima broadly coincide with the regions of active convection; however, a slight but significant mismatch is found between the two. This mismatch indicates that T-CPT is not directly formed and maintained by tropical deep convection (Highwood and Hoskins 1998; Seidel et al. 2001). The spatial structure of the annual-mean P-CPT, which has been sparsely reported using multiyear high-resolution observations, shows an almost homogeneous pattern in the tropics, except over the Tibetan Plateau and South Pacific. This feature is somewhat different from the lapse rate tropopause pressure, which exhibits weak but nonnegligible zonal structure in the deep tropics (see Fig. 5a of Son et al. 2011). It turns out that the CPT is so sharp that the level (height) of the CPT is barely modified by local processes such as deep

convection and zonally asymmetric tropospheric circulation in seasonal or interannual time scales. The homogeneity of P-CPT justifies CPT analysis at fixed or interpolated level, which has been often conducted with reanalysis and numerical model data (e.g., Zhou et al. 2001b; Gettelman et al. 2010): it does not introduce a significant bias in spatial pattern. However, caution is still needed in the analysis because fixed-level analysis does tend to smooth CPT variability. S-CPT, which is defined by static stability change across the CPT, is dominated by static stability (more specifically temperature lapse rate) right above the CPT and shows a very similar annual-mean structure to T-CPT, although the latitudinal extent of S-CPT is narrow and confined within the deep tropics.

It is further found that spatial structure of the annual-mean CPT properties is largely due to the boreal winter CPT, which is colder, higher (lower in pressure), and sharper than the summer CPT. This seasonality is caused by a temperature anomaly near the CPT [~(70–90) hPa], which undergoes strong seasonal cycle likely caused by both Brewer–Dobson circulation and local wave forcing. In addition, a nonzonality is present in the seasonal cycle of T-CPT. The amplitude of the seasonal cycle is strong in the western Pacific and noticeably weak in the mideastern Pacific and in the Atlantic. These are attributed to large-scale zonal circulations in the tropics, such as the Walker circulation (Zhou et al. 2001b; Fueglistaler et al. 2009); however, strong coincidence between warm T-CPT and 100-hPa westerly wind during boreal winter suggests a possible contribution by tropical or extratropical eddies in maintaining regional CPT properties.

Intraseasonal variabilities of T-CPT and P-CPT, which are defined by monthly standard deviation, are relatively weak in the tropics where short-term variability of deep convection is maximal. In addition, they are largely homogeneous in the zonal direction, with no distinct local maxima. These results, however, do not indicate no effect of deep convection on intraseasonal variability of CPT properties. In fact, intraseasonal variability of equatorial CPT properties is largely caused by Kelvin waves and MJO convection. T-CPT anomalies with a slightly faster phase speed compared to those of OLR suggest that T-CPT anomalies are strongly modulated by free (or internal) Kelvin waves. The T-CPT anomalies at the MJO band have a relatively smaller zonal scale (maximum power at wavenumber 3) compared to OLR anomalies (maximum power at wavenumber 1) because of their longer persistence. In contrast to T-CPT and P-CPT, intraseasonal variability of S-CPT shows a significant longitudinal structure and seasonality. This difference can be explained by convectively coupled waves, especially equatorial waves that propagate along the equator with convection: their vertically tilted temperature anomaly effectively changes the temperature lapse rate around the CPT.

In this study, interannual variability and long-term trend are not analyzed because the analysis period is only 4 yr. The interannual variability of the CPT is known to be related to the QBO (e.g., Zhou et al. 2001a; Randel et al. 2003; Schmidt et al. 2004) and ENSO (e.g., Zhou et al. 2001a; Randel et al. 2000, for LRT). In fact, QBO events are noticeable in Fig. 6 (stronger warm anomaly found in 2008 and 2010, spring to summer), and the 2010 El Niño event could be related to the relatively zonal structure of T-CPT found in Fig. 7a. Because T-CPT is closely related to the amount of stratospheric water vapor on interannual to decadal time scales (e.g., Randel et al. 2004; Fueglistaler and Haynes 2005), long-term variability and trend of T-CPT could be important in understanding stratospheric water vapor and related UTLS processes. We expect further operation of GPS radio occultation systems will provide useful information for understanding and addressing these issues.

Acknowledgments. We thank UCAR CDAAC for providing COSMIC data via their website (at http://www.cosmic.ucar.edu/). The NOAA OLR and ERA-Interim data were provided by the NOAA/ESRL, and ECMWF, respectively, from their websites. We also thank three anonymous reviewers for constructive comments. This study is funded in part by the KMA R&D program under Grant RACS 2010-2017. The author J. K. is also partly supported by Global Environmental and Climate Change Center (GEC3) graduate student stipend.

REFERENCES

Anthes, R. A., and Coauthors, 2008: The COSMIC/FORMOSAT-3 mission: Early results. *Bull. Amer. Meteor. Soc.,* **89,** 313–333.

Birner, T., 2006: Fine-scale structure of the extratropical tropopause region. *J. Geophys. Res.,* **111,** D04104, doi:10.1029/2005JD006301.

——, A. Dörnbrack, and U. Schumann, 2002: How sharp is the tropopause at midlatitudes? *Geophys. Res. Lett.,* **29,** 1700, doi:10.1029/2002GL015142.

Boehm, M. T., and S. Lee, 2003: The implications of tropical Rossby waves for tropical tropopause cirrus formation and for the equatorial upwelling of the Brewer–Dobson circulation. *J. Atmos. Sci.,* **60,** 247–261.

Brewer, A., 1949: Evidence for a world circulation provided by the measurements of helium and water vapour distribution in the stratosphere. *Quart. J. Roy. Meteor. Soc.,* **75,** 351–363.

de F. Forster, P. M., and K. P. Shine, 1999: Stratospheric water vapour changes as a possible contributor to observed stratospheric cooling. *Geophys. Res. Lett.,* **26,** 3309–3312.

Dima, I. M., J. M. Wallace, and I. Kraucunas, 2005: Tropical zonal momentum balance in the NCEP reanalyses. *J. Atmos. Sci.,* **62,** 2499–2513.

Durre, I., R. S. Vose, and D. B. Wuertz, 2006: Overview of the integrated global radiosonde archive. *J. Climate,* **19,** 53–68.

Eguchi, N., and M. Shiotani, 2004: Intraseasonal variations of water vapor and cirrus clouds in the tropical upper troposphere. *J. Geophys. Res.,* **109,** D12106, doi:10.1029/2003JD004314.

Fueglistaler, S., and P. H. Haynes, 2005: Control of interannual and longer-term variability of stratospheric water vapor. *J. Geophys. Res.,* **110,** D24108, doi:10.1029/2005JD006019.

——, A. E. Dessler, T. J. Dunkerton, I. Folkins, Q. Fu, and P. W. Mote, 2009: Tropical tropopause layer. *Rev. Geophys.,* **47,** RG1004, doi:10.1029/2008RG000267.

Gettelman, A., and T. Birner, 2007: Insights into tropical tropopause layer processes using global models. *J. Geophys. Res.,* **112,** D23104, doi:10.1029/2007JD008945.

——, W. J. Randel, F. Wu, and S. T. Massie, 2002a: Transport of water vapor in the tropical tropopause layer. *Geophys. Res. Lett.,* **29,** 1009, doi:10.1029/2001GL013818.

——, M. L. Salby, and F. Sassi, 2002b: Distribution and influence of convection in the tropical tropopause region. *J. Geophys. Res.,* **107,** 4080, doi:10.1029/2001JD001048.

——, and Coauthors, 2009: The tropical tropopause layer 1960–2100. *Atmos. Chem. Phys.,* **9,** 1621–1637.

——, and Coauthors, 2010: Multimodel assessment of the upper troposphere and lower stratosphere: Tropics and global trends. *J. Geophys. Res.,* **115,** D00M08, doi:10.1029/2009JD013638.

Gorbunov, M. E., and K. B. Lauritsen, 2004: Analysis of wave fields by Fourier integral operators and their application for radio occultations. *Radio Sci.,* **39,** RS4010, doi:10.1029/2003RS002971.

Grise, K. M., D. W. J. Thompson, and T. Birner, 2010: A global survey of static stability in the stratosphere and upper troposphere. *J. Climate,* **23,** 2275–2292.

Hartmann, D. L., J. R. Holton, and Q. Fu, 2001: The heat balance of the tropical tropopause, cirrus, and stratospheric dehydration. *Geophys. Res. Lett.,* **28,** 1969–1972.

Haynes, P., M. McIntyre, T. Shepherd, C. Marks, and K. Shine, 1991: On the ''downward control'' of extratropical diabatic circulations by eddy-induced mean zonal forces. *J. Atmos. Sci.,* **48,** 651–679.

He, W., S.-P. Ho, H. Chen, X. Zhou, D. Hunt, and Y.-H. Kuo, 2009: Assessment of radiosonde temperature measurements in the upper troposphere and lower stratosphere using COSMIC radio occultation data. *Geophys. Res. Lett.,* **36,** L17807, doi:10.1029/2009GL038712.

Highwood, E., and B. Hoskins, 1998: The tropical tropopause. *Quart. J. Roy. Meteor. Soc.,* **124,** 1579–1604.

Holton, J. R., P. H. Haynes, M. E. McIntyre, A. R. Douglass, R. B. Rood, and L. Pfister, 1995: Stratosphere-troposphere exchange. *Rev. Geophys.,* **33,** 403–439.

Jensen, A. S., M. S. Lohmann, H.-H. Benzon, and A. S. Nielsen, 2003: Full Spectrum Inversion of radio occultation signals. *Radio Sci.,* **38,** 1040, doi:10.1029/2002RS002763.

Kerr-Munslow, M., and W. A. Norton, 2006: Tropical wave driving of the annual cycle in tropical tropopause temperatures. Part I: ECMWF analyses. *J. Atmos. Sci.,* **63,** 1410–1419.

Kiladis, G., K. Straub, G. Reid, and K. Gage, 2001: Aspects of interannual and intraseasonal variability of the tropopause and lower stratosphere. *Quart. J. Roy. Meteor. Soc.,* **127,** 1961–1983.

Kishore, P., S. P. Namboothiri, K. Igarashi, J. H. Jiang, C. O. Ao, and L. J. Romans, 2006: Climatological characteristics of the tropopause parameters derived from GPS/CHAMP and GPS/SAC-C measurements. *J. Geophys. Res.,* **111,** D20110, doi:10.1029/2005JD006827.

——, ——, J. H. Jiang, V. Sivakumar, and K. Igarashi, 2009: Global temperature estimates in the troposphere and stratosphere: A validation study of COSMIC/FORMOSAT-3 measurements. *Atmos. Chem. Phys.,* **9,** 897–908, doi:10.5194/acp-9-897-2009.

Kuang, Z., and C. S. Bretherton, 2004: Convective influence on the heat balance of the tropical tropopause layer: A cloud-resolving model study. *J. Atmos. Sci.,* **61,** 2919–2927.

Kursinski, E. R., G. A. Hajj, J. T. Schofield, R. P. Linfield, and K. R. Hardy, 1997: Observing Earth's atmosphere with radio occultation measurements using the global positioning system. *J. Geophys. Res.,* **102D,** 23 429–23 465.

Lee, S., 1999: Why are the climatological zonal winds easterly in the equatorial upper troposphere? *J. Atmos. Sci.,* **56,** 1353–1363.

Liebmann, B., and C. A. Smith, 1996: Description of a complete (interpolated) outgoing longwave radiation dataset. *Bull. Amer. Meteor. Soc.,* **77,** 1275–1277.

Mote, P. W., and Coauthors, 1996: An atmospheric tape recorder: The imprint of tropical tropopause temperatures on stratospheric water vapor. *J. Geophys. Res.,* **101D,** 3989–4006.

——, T. J. Dunkerton, M. E. Mclntyre, E. A. Ray, P. H. Haynes, and J. M. Russell III, 1998: Vertical velocity, vertical diffusion, and dilution by midlatitude air in the tropical lower stratosphere. *J. Geophys. Res.,* **103D,** 8651–8666.

——, H. L. Clark, T. J. Dunkerton, R. S. Harwood, and H. C. Pumphrey, 2000: Intraseasonal variations of water vapor in the tropical upper troposphere and tropopause region. *J. Geophys. Res.,* **105D,** 17 457–17 470.

Nishida, M., A. Shimizu, and T. Tsuda, 2000: Seasonal and longitudinal variations in the tropical tropopause observed with the GPS occultation technique (GPS/MET). *J. Meteor. Soc. Japan,* **78,** 691–700.

Norton, W. A., 2006: Tropical wave driving of the annual cycle in tropical tropopause temperatures. Part II: Model results. *J. Atmos. Sci.,* **63,** 1420–1431.

Randel, W. J., and F. Wu, 2005: Kelvin wave variability near the equatorial tropopause observed in GPS radio occultation measurements. *J. Geophys. Res.,* **110,** D03102, doi:10.1029/2004JD005006.

——, ——, and D. J. Gaffen, 2000: Interannual variability of the tropical tropopause derived from radiosonde data and NCEP reanalyses. *J. Geophys. Res.,* **105D,** 15 509–15 523.

——, R. R. Garcia, and F. Wu, 2002: Time-dependent upwelling in the tropical lower stratosphere estimated from the zonal-mean momentum budget. *J. Atmos. Sci.,* **59,** 2141–2152.

——, F. Wu, and W. R. Rios, 2003: Thermal variability of the tropical tropopause region derived from GPS/MET observations. *J. Geophys. Res.,* **108,** 4024, doi:10.1029/2002JD002595.

——, ——, S. J. Oltmans, K. Rosenlof, and G. E. Nedoluha, 2004: Interannual changes of stratospheric water vapor and correlations with tropical tropopause temperatures. *J. Atmos. Sci.,* **61,** 2133–2148.

——, R. Garcia, and F. Wu, 2008: Dynamical balances and tropical stratospheric upwelling. *J. Atmos. Sci.,* **65,** 3584–3595.

Reid, G. C., and K. S. Gage, 1981: On the annual variation in height of the tropical tropopause. *J. Atmos. Sci.,* **38,** 1928–1938.

Schmidt, T., J. Wickert, G. Beyerle, and C. Reigber, 2004: Tropical tropopause parameters derived from GPS radio occultation measurements with CHAMP. *J. Geophys. Res.,* **109,** D13105, doi:10.1029/2004JD004566.

——, S. Heise, J. Wickert, G. Beyerle, and C. Reigber, 2005: GPS radio occultation with CHAMP and SAC-C: Global monitoring of thermal tropopause parameters. *Atmos. Chem. Phys.,* **5,** 1473–1488, doi:10.5194/acp-5-1473-2005.

Seidel, D. J., R. Ross, J. K. Angell, and G. C. Reid, 2001: Climatological characteristics of the tropical tropopause as revealed by radiosondes. *J. Geophys. Res.,* **106D,** 7857–7878.

Shepherd, T. G., 2002: Issues in stratosphere-troposphere coupling. *J. Meteor. Soc. Japan,* **80,** 769–792, doi:10.2151/jmsj.80.769.

Sherwood, S. C., T. Horinouchi, and H. A. Zeleznik, 2003: Convective impact on temperatures observed near the tropical tropopause. *J. Atmos. Sci.,* **60,** 1847–1856.

Simmons, A., S. Uppala, D. Dee, and S. Kobayashi, 2007: ERA-Interim: New ECMWF reanalysis products from 1989 onwards. *ECMWF Newsletter,* No. 110, ECMWF, Reading, United Kingdom, 25–35.

Solomon, S., K. H. Rosenlof, R. W. Portmann, J. S. Daniel, S. M. Davis, T. J. Sanford, and G.-K. Plattner, 2010: Contributions of stratospheric water vapor to decadal changes in the rate of global warming. *Science,* **327,** 1219–1223, doi:10.1126/science.1182488.

Son, S.-W., and S. Lee, 2007: Intraseasonal variability of the zonal-mean tropical tropopause height. *J. Atmos. Sci.,* **64,** 2695–2706.

——, N. F. Tandon, and L. M. Polvani, 2011: The fine-scale structure of the global tropopause derived from COSMIC GPS radio occultation measurements. *J. Geophys. Res.,* **116,** D20113, doi:10.1029/2011JD016030.

Suzuki, J., and M. Shiotani, 2008: Space-time variability of equatorial Kelvin waves and intraseasonal oscillations around the tropical tropopause. *J. Geophys. Res.,* **113,** D16110, doi:10.1029/2007JD009456.

Wheeler, M., and G. N. Kiladis, 1999: Convectively coupled equatorial waves: Analysis of clouds and temperature in the wavenumber–frequency domain. *J. Atmos. Sci.,* **56,** 374–399.

——, ——, and P. J. Webster, 2000: Large-scale dynamical fields associated with convectively coupled equatorial waves. *J. Atmos. Sci.,* **57,** 613–640.

Yulaeva, E., J. R. Holton, and J. M. Wallace, 1994: On the cause of the annual cycle in tropical lower-stratospheric temperatures. *J. Atmos. Sci.,* **51,** 169–169.

Zhou, X., and J. R. Holton, 2002: Intraseasonal variations of tropical cold-point tropopause temperatures. *J. Climate,* **15,** 1460–1473.

——, M. A. Geller, and M. Zhang, 2001a: Cooling trend of the tropical cold point tropopause temperatures and its implications. *J. Geophys. Res.,* **106D,** 1511–1522.

——, ——, and ——, 2001b: Tropical cold point tropopause characteristics derived from ECMWF reanalyses and soundings. *J. Climate,* **14,** 1823–1838.